Capillary Forces: Influence of Roughness and Heterogeneity

Hans-Jürgen Butt*

Max-Planck-Institute for Polymer Research, Ackermannweg 10, 55128 Mainz, Germany

Received November 21, 2007. In Final Form: February 5, 2008

A formalism is described to calculate capillary forces between solid surfaces analytically. Assumptions are that the liquid menisci (1) have a much larger extension parallel to the gap than normal and (2) are formed by capillary condensation and are in equilibrium with the vapor. To calculate capillary forces, first the gap between the two surfaces is described by a height distribution function. Roughness is considered with an asperity distribution function. Both distributions can at least in principal be measured by light, electron, or atomic force microscopy or grazing incidence X-ray reflectivity. The total capillary force versus distance or vapor pressure is obtained by a convolution of both distributions and an integration. The formalism is applied to calculate the capillary force between rough spherical particles. In addition, a method to consider surface heterogeneity is suggested.

Introduction

Liquid menisci formed between two solid surfaces cause an attractive force, the capillary force. Capillary forces influence and often dominate a wide range of phenomena. Examples are the flow of granular materials,[1−3] the aggregation of particles in binary liquid mixtures,[4−6] the adhesion of insects or Geckos to surfaces,[7] friction between two solid surfaces,[8,9] sintering of ceramic or metallic particles,[10] and the stiction of the head on a magnetic storage disk.[11−13]

In many cases, a meniscus is formed by capillary condensation. Capillary condensation of water will inevitably occur between two hydrophilic surfaces in contact and under ambient conditions. Capillary condensation is described by the Kelvin equation. For the condensation of liquid into a narrow gap formed by two lyophilic solid surfaces and for rotationally symmetric geometry (Figure 1), the Kelvin equation is

$$-\frac{\ln(P/P_0)}{\lambda_K} = \frac{1}{r} - \frac{1}{l} \text{ with } \lambda_K = \frac{\gamma V_m}{k_B T} \qquad (1)$$

Here, r is the meridional radius of curvature of the liquid−vapor interface of the meniscus normal to the surface and l is the azimuthal curvature parallel to the surfaces. P is the vapor pressure, P_0 is the saturation vapor pressure, V_m is the molecular volume of the molecules in the liquid phase, k_B is Boltzmann's constant, and T is the temperature. The constant λ_K, which I call the Kelvin length, characterizes the length scale for capillary condensation. For water and toluene, the Kelvin lengths are 0.523 and 1.20 nm at 298 K, respectively.

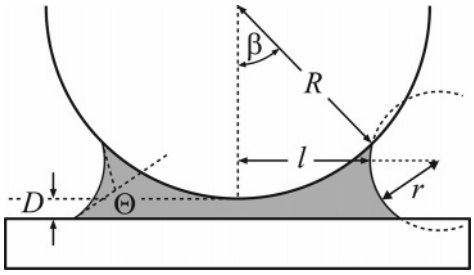

Figure 1. Schematic drawing of a sphere interacting with a plate via a liquid meniscus (gray). Symbols used in the text are indicated.

To calculate capillary forces, different numerical approaches have been suggested and compared to analytical approximations.[14−17] The shape of the liquid meniscus needs to be calculated from the Laplace equation assuming constant curvature of the liquid−vapor interface.[18,19] Once the shape of the meniscus is known, the force is calculated by multiplying the cross-sectional area by the Laplace pressure and adding the surface tension of the liquid multiplied by the circumference.[1,20] Even for simple geometries no precise analytical equations for the capillary force can be given. For small menisci and rotationally symmetric geometries, the toroidal approximation can be applied.[1,20] In the toroidal (sometimes also called circular) approximation, the radius of curvature normal to the two interacting solid surfaces is assumed to be described by a circle of radius r. The shape, however, is not precisely a circle but a nodoid.[19] For small menisci where the effect of gravity can be neglected, the toroidal approximation is applicable, and deviations between forces calculated numerically with the precise shape agree with the results of the toroidal approximation.[18,21−24] Using the toroidal approximation, the force for several simple geometries has been calculated.[18,21,22,24−26]

* E-mail: butt@mpip-mainz.mpg.de. Fax: +49-6131-379-310. Phone: +49-6131-379-111.

(1) Haines, W. B. *J. Agric. Sci.* **1927**, *17*, 264−290.
(2) Bocquet, L.; Charlaix, E.; Ciliberto, S.; Crassous, J. *Nature* **1998**, *396*, 735−737.
(3) Herminghaus, S. *Adv. Phys.* **2005**, *54*, 221−261.
(4) Bloomquist, C. R.; Shutt, R. S. *Ind. Eng. Chem.* **1940**, *32*, 827−831.
(5) Eggleton, A. E. J.; Puddington, I. E. *Can. J. Chem.* **1954**, *32*, 86−93.
(6) Löwen, H. *Phys. Rev. Lett.* **1995**, *74*, 1028−1031.
(7) Qian, J.; Gao, H. *Acta Biomater.* **2006**, *2*, 51−58.
(8) Cottin-Bizonne, C.; Jurine, S.; Baudry, J.; Crassous, J.; Restagno, F.; Charlaix, E. *Eur. Phys. J. E* **2002**, *9*, 47−53.
(9) Riedo, E.; Palaci, I.; Boragno, C.; Brune, H. *J. Phys. Chem. B* **2004**, *108*, 5324−5328.
(10) Huppmann, W. J.; Riegger, H. *Acta Metall.* **1975**, *23*, 965−971.
(11) Mate, C. M. *J. Appl. Phys.* **1992**, *72*, 3084−3090.
(12) Tian, H.; Matsudaira, T. *ASME J. Tribol.* **1993**, *115*, 28−35.
(13) Gao, C.; Bhushan, B. *Wear* **1995**, *190*, 60−75.
(14) Marmur, A. *Langmuir* **1993**, *9*, 1922−1926.
(15) de Lazzer, A.; Dreyer, M.; Rath, H. J. *Langmuir* **1999**, *15*, 4551−4559.
(16) Gao, C. *Appl. Phys. Lett.* **1997**, *71*, 1801−1803.
(17) Bauer, C.; Bieker, T.; Dietrich, S. *Phys. Rev. E* **2000**, *62*, 5324−5338.
(18) Melrose, J. C.; Wallick, G. C. *J. Phys. Chem.* **1967**, *71*, 3676−3678.
(19) Iinoya, K.; Asakawa, S.; Hotta, K.; Burson, J. H. *Powder Technol.* **1967**, *1*, 28−32.
(20) Fisher, R. A. *J. Agric. Sci.* **1926**, *16*, 492−505.
(21) Heady, R. B.; Cahn, J. W. *Metall. Trans.* **1970**, *1*, 185−189.
(22) Orr, F. M.; Scriven, L. E.; Rivas, A. P. *J. Fluid Mech.* **1975**, *67*, 723−742.
(23) de Bisschop, F. R. E.; Rigole, W. J. L. *J. Colloid Interface Sci.* **1982**, *88*, 117−165.
(24) Lian, G.; Thornton, C.; Adams, M. J. *J. Colloid Interface Sci.* **1993**, *161*, 138−147.
(25) Clark, W. C.; Haynes, J. M.; Mason, G. *Chem. Eng. Sci.* **1968**, *23*, 810−812.

10.1021/la703640f CCC: $40.75
Published on Web 04/29/2008

Even then the equations are not explicit with respect to distance or vapor pressure. Although this is only a nuisance when fitting force versus distance curves, it turns into a real problem when trying to describe more complex systems such as granular matter.

Surface roughness poses a further difficulty. The Kelvin length determines the length scale for capillary forces. Because surfaces are usually rough on the 1 nm scale, surface roughness will critically influence the capillary force.[27,28] Several authors take roughness into account by introducing a single asperity.[29−33] Halsey and Levine[34] and Bocquet et al.[2] extended this approach to describe interacting spheres by discriminating three regimes: In the asperity regime, for low relative vapor pressure P/P_0 and thus small liquid volumes, the capillary force is dominated by a single asperity. For intermediate vapor pressure, more and more liquid bridges form, and the roughness dominates. At high vapor pressure, the overall radius of the particles dominates. Greenwood and Williamson described surface roughness by a distribution of spherical asperities.[35] Their approach was later used to describe capillary forces between rough surfaces covered with thin nonvolatile liquids.[12,36,37] The effect of roughness caused by regularly placed, elastically deformable hemispheres was calculated by Farshchi et al.[32] To describe the velocity dependence of friction forces, Riedo et al.[9] take roughness into account simply by assuming that capillary bridges form at a number of asperities.

One aspect, which is intensely debated with respect to wetting and adsorption phenomena[38] but has to my knowledge never been introduced into the discussion of capillary forces, is surface heterogeneity. Solid surfaces are usually not perfectly homogeneous. Different crystal surfaces are exposed, and defects and variations in the chemical composition lead to local changes in the contact angle. This can influence the capillary force.

Here, I propose a simple formalism to calculate capillary forces between solid surfaces including roughness. The formalism allows the consideration of any statistical distribution of surface roughness without assuming a certain asperity shape. It also allows the integration of the treatment of surface heterogeneity. The main assumption is that the liquid menisci extend laterally (parallel to the apparent surfaces) over much larger distances than the distance normal to the surfaces. For the rotationally symmetric case, this implies that $l \gg r$ (Figure 1). A further assumption is that menisci form by capillary condensation and that the system is in equilibrium with respect to condensation and evaporation. I ignore the effect of other surface forces that may have a direct influence on the force and also might change the wetting properties.[39] As a continuum approach, it also ignores the discrete molecular nature of all materials involved.

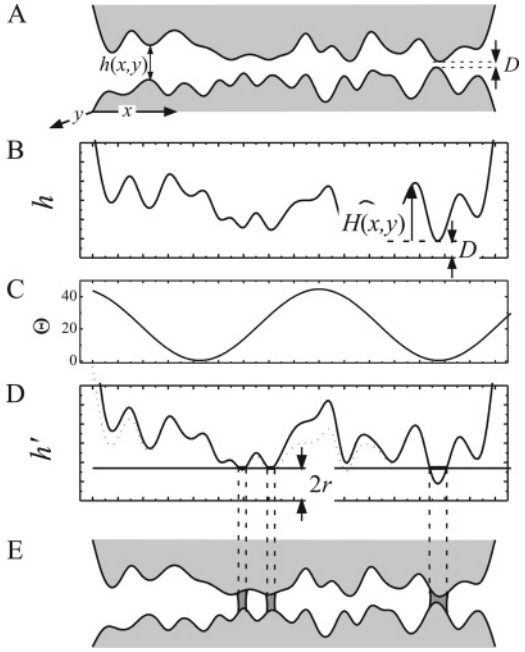

Figure 2. Schematic drawing of two surfaces that are separated by an irregular gap. A cut in the x direction is shown (A). The surfaces of the interacting solids are 3D objects, and the gap is described by a separation function $h(x, y)$ (B). The h scale is largely extended as compared to the x scale. In the example, surface heterogeneity, as characterized by the contact angle, was assumed to change periodically between zero and 45° (C). It was further supposed that $\Theta(x, y) = \Theta_1(x, y) = \Theta_2(x, y)$. The effective separation $h' = 2h/(\cos\Theta_1 + \cos\Theta_2)$ determines whether a meniscus is formed in equilibrium (D). For comparison, h is plotted as a dashed line in part D. A meniscus is stable if $h' \leq 2r$, with r being determined by the vapor pressure via Kelvin's equation (E).

Theory

General Model. The aim is to calculate the capillary force between two undeformable surfaces of arbitrary shape (Figure 2A). Let $h(x, y)$ be the separation between the two surfaces at lateral position (x, y) (Figure 2B). The separation consists of a shape-dependent part, $H(x,y)$, and the distance D according to $h(x, y) = H(x, y) + D$. $H(x, y)$ is the separation at zero distance. The distance D is the smallest separation in the area considered. The surface properties are quantified by the contact angles of the top and bottom surfaces, $\Theta_1(x, y)$ and $\Theta_2(x, y)$, respectively. Both contact angles are $<90°$ at all (x, y); otherwise, no meniscus would form at all. For a periodically varying contact angle in the x direction, this is shown in Figure 2C.

Two main assumptions are made: First, menisci are formed by capillary condensation and are in equilibrium with their vapor phase. Thus, Kelvin's equation is valid. Second, the lateral extension of the menisci bridging the two surfaces is much greater than the separation; please note that the h scale in Figure 2 is largely extended as compared to the lateral dimensions. Then the curvature normal to the surfaces, $1/r$, is much higher than the curvature perpendicular to it, $1/l$, and the total curvature, $1/r \approx 1/r - 1/l$, is dominated by $1/r$. If both assumptions are fulfilled, then radius r is linked to the vapor pressure by the simplified Kelvin equation

$$r = -\frac{\lambda_K}{\ln(P/P_0)} \tag{2}$$

The capillary force of a liquid meniscus consists of two contributions:[20,40] The Laplace pressure is multiplied by the cross-

(26) Tselishchev, Y. G.; Val'tsifer, V. A. *Colloid J.* **2003**, *65*, 385−389.
(27) Colbeck, S. C. *J. Adhesion Sci. Technol.* **1997**, *11*, 359−371.
(28) Butt, H.-J.; Farshchi-Tabrizi, M.; Kappl, M. *J. Appl. Phys.* **2006**, *100*, 024312.
(29) Pietsch, W.; Rumpf, H.; Haftkraft, K. *Chem. Ing. Tech.* **1967**, *39*, 885−893.
(30) Gulbinski, W.; Pailharey, D.; Suszko, T.; Mathey, Y. *Surf. Sci.* **2001**, *475*, 149−158.
(31) Rabinovich, Y. I.; Esayanur, M. S.; Johanson, K. D.; Adler, J. J.; Moudgil, B. M. *J. Adhes. Sci. Technol.* **2002**, *16*, 887−903.
(32) Farshchi, M.; Kappl, M.; Cheng, Y.; Gutmann, J. S.; Butt, H.-J. *Langmuir* **2006**, *22*, 2171−2184.
(33) Paajanen, M.; Katainen, J.; Pakarinen, O. H.; Foster, A. S.; Lahtinen, J. *J. Colloid Interface Sci.* **2006**, *304*, 518−523.
(34) Halsey, T. C.; Levine, A. J. *Phys. Rev. Lett.* **1998**, *80*, 3141−3145.
(35) Greenwood, J. A.; Williamson, J. B. P. *Proc. Royal Soc. London* **1966**, A *295*, 300−319.
(36) Li, Y.; Talke, F. E. *Tribology and Mechanics of Magnetic Strorage Systems* **1990**, *SP 27*, 79−84.
(37) Koka, R.; Viswanathan, K. V.; Rothschild, W. *Adv. Info. Storage Syst., ASME* **1991**, *3*, 117−126.
(38) Adamson, A. W. *Physical Chemistry of Surfaces*; John Wiley & Sons: New York: 1990; p 784.
(39) Charlaix, E.; Crassous, J. *J. Chem. Phys.* **2005**, *122*, 184701.
(40) Princen, H. M. *J. Colloid Interface Sci.* **1968**, *26*, 249−253.

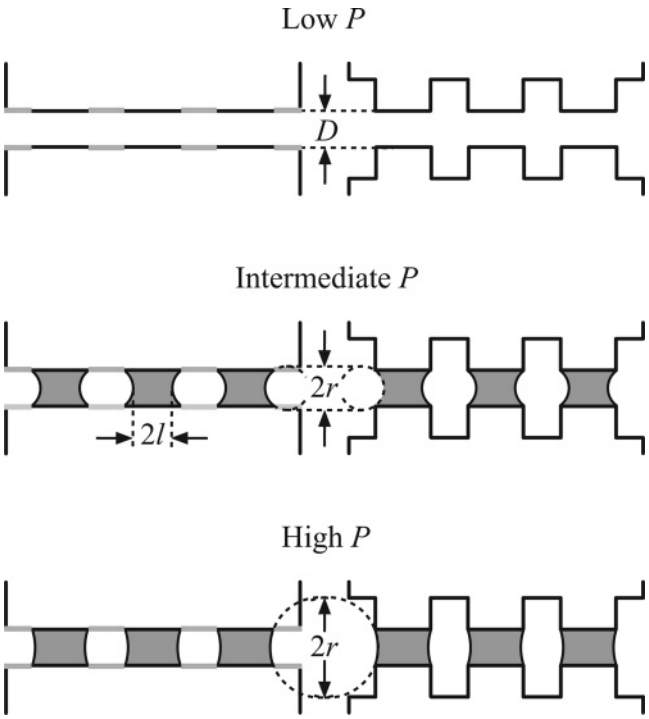

Figure 3. Schematic of a liquid condensing between two differently textured parallel plates. On the left, the surfaces are smooth and lyophobic (gray) with lyophilic (black) patches. On the right, the plates are lyophilic throughout but have elevated regions. With respect to liquid condensation, both gaps show the same behavior. The scale normal to the gap is largely extended.

sectional area A, and the surface tension is multiplied by the circumference. For $r \ll l$, the total capillary force is dominated by the Laplace pressure, and it can be expressed as[12,34]

$$F = A\frac{\gamma}{r} \tag{3}$$

A liquid condenses into a gap when the gap width is smaller than $2cr$, where c is the mean cosine of the contact angles of the two surfaces. Thus, the condition for the formation of a liquid meniscus is

$$h(x, y, D) = H(x, y) + D \le 2cr \text{ with } c(x, y) = \frac{\cos\Theta_1(x, y) + \cos\Theta_2(x, y)}{2} \tag{4}$$

The quantity $2cr$ is the distance that a circular arc can span assuming the contact angles to be Θ_1 and Θ_2. To visualize eq 4, it is instructive to define an effective separation $h' = h/c$. If we plot $h'(x, y)$, then all those parts below $2r$ will form a meniscus (Figure 2D). A is simply the area below the plane defined by $2r$. Equation 4 is derived by assuming that the surfaces are not strongly inclined.

Equation 4 shows that surface topography and local wettability can be treated in similar ways with respect to the formation of capillary bridges. The only relevant quantity is the combination of both as expressed by the effective separation. This similarity is demonstrated for two parallel plates in Figure 3. On the left, the surfaces are smooth but heterogeneous. On a lyophobic surface ($\Theta > 90°$), a pattern of lyophilic patches ($\Theta = 0°$) is distributed. At low vapor pressure, no menisci will form. Once the vapor pressure has reached $P = P_0 \exp(-2\lambda_K/D)$, liquid will condense into the gap. Further increases in the vapor pressure increase the

(41) Reference deleted in proof.

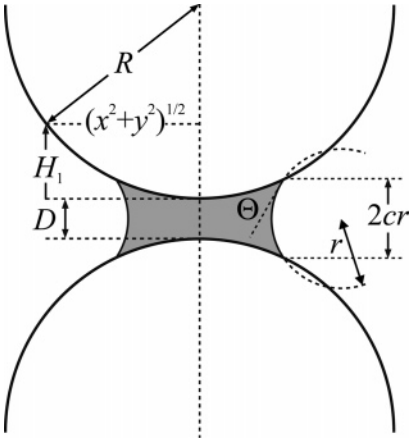

Figure 4. Schematic of two equal spheres interacting with each other via a liquid meniscus.

radius of curvature r. Precisely the same menisci form between completely lyophilic surfaces with elevated patches of the same size as the lyophilic regions.

Constant Contact Angle. Now I assume that the contact angles of the surfaces are constant. For a given geometry of the interacting surfaces, A can be expressed as a function of only one "height" coordinate: $A(z)$ is the cross-sectional area for which $H(x, y) \le z$. In Figure 2D, this area is highlighted. The capillary force is

$$F = A(2cr - D)\frac{\gamma}{r} \text{ for } D \le 2cr \tag{5}$$

and $F = 0$ for $D > 2cr$.

It is instructive to express $A(z)$ by $A(z) = A_0G(z)$. Here, A_0 is a reference area, which should be at least as large as the range of the maximal meniscus. Usually, it is the total apparent area considered. $G(z)$ is the integrated height distribution. It is related to the height distribution $g(z)$, which is the probability of finding a certain effective height z in the interval $z \ldots z + \mathrm{d}z$. The height distribution g is in units of m^{-1} and normalized: $\int_0^\infty g(z)\,\mathrm{d}z = 1$. Both are related by

$$G(z) = \int_0^z g(\zeta)\,\mathrm{d}\zeta \text{ and } g(z) = \frac{\mathrm{d}G}{\mathrm{d}z} = \frac{1}{A_0}\frac{\mathrm{d}A}{\mathrm{d}z} \tag{6}$$

The integrated height distribution varies between $G(z \to 0) = 0$ and $G(z \to \infty) = 1$. Equation 5 can be expressed as

$$F = A_0G(2cr - D)\frac{\gamma}{r} \tag{7}$$

Two Equal Smooth Spheres. As an example, I consider two equal spheres of radii R and contact angle Θ interacting with each other (Figure 4). The shape H can be expressed as $H = 2H_1$, where H_1 is the height function of an individual sphere. The maximal value of H is $H_{max} = 2R$. With $R^2 = (R - H_1)^2 + (x^2 + y^2) \Rightarrow 2RH_1 = H_1^2 + (x^2 + y^2)$, we can express the cross-sectional area $A = \pi(x^2 + y^2)$ by $A = \pi(RH - H^2/4)$. Then

$$g(z) = \frac{1}{\pi R^2}\frac{\mathrm{d}A}{\mathrm{d}z} = \frac{1}{R^2}\left(R - \frac{z}{2}\right) \tag{8}$$

$$G(z) = \frac{1}{R^2}\int_0^z \left(R - \frac{\zeta}{2}\right)\mathrm{d}\zeta = \frac{1}{R^2}\left(Rz - \frac{z^2}{4}\right) \tag{9}$$

With $A_0 = \pi R^2$, the capillary force according to eq 7 is

$$F = \pi\gamma R\left[2c - \frac{D}{r} - \frac{(2cr - D)^2}{4rR}\right] \tag{10}$$

Because $R \gg r, D$ we can neglect the last term and

$$F = \pi\gamma R\left(2c - \frac{D}{r}\right) \tag{11}$$

Two Different Smooth Spheres. If the radii of the two spheres R_1 and R_2 are different (R_1 is assumed to be the smaller sphere, $R_1 \leq R_2$), then shape H is given by $H = H_1 + H_2$ with $H_1 = R_1 - \sqrt{{R_1}^2-(x^2+y^2)}$ and $H_2 = R_2 - \sqrt{{R_2}^2-(x^2+y^2)}$. In the vicinity of the contact ($\sqrt{(x^2+y^2)} \ll R_1$), we can approximate H by $H = R^* - \sqrt{{R^*}^2-(x^2+y^2)}$. Here, $R^* = R_1R_2/(R_1 + R_2)$ is the effective radius. We can express the cross-sectional area $A = \pi(x^2 + y^2)$ by $A = \pi(2R^*H - H^2)$. The maximal cross-sectional area is $\pi{R_1}^2$. It is safe to assume that forces outside the range $\sqrt{(x^2+y^2)} \leq R_1/2$ are negligible. Therefore, we are free to choose $A_0 = \pi{R^*}^2$ as the reference area. Forces outside that area will not contribute significantly. Then

$$g(z) = \frac{1}{\pi{R^*}^2}\frac{\mathrm{d}A}{\mathrm{d}z} = \frac{2}{{R^*}^2}(R^* - z) \tag{12}$$

$$G(z) = \frac{2}{{R^*}^2}\int_0^z (R^* - \varsigma)\,\mathrm{d}\xi = \frac{2}{{R^*}^2}\left(R^*z - \frac{z^2}{2}\right) \tag{13}$$

According to eq 7, the capillary force is

$$F = \pi R^*\gamma\left[4c - \frac{2D}{r} - \frac{(2cr - D)^2}{rR^*}\right] \tag{14}$$

Because $R^* \gg r, D$ we can neglect the last term and

$$F = 2\pi\gamma R^*\left(2c - \frac{D}{r}\right) \tag{15}$$

This agrees with the approximation of Derjaguin.[42]

Figure 5 shows capillary forces versus distance and force versus vapor pressure curves, calculated with eq 15 compared to "exact" solutions. As an example, I chose a sphere of radius ($R_1 = 2\,\mu$m) interacting with a plane ($R_2 = \infty$), in which case $R^* = R_1$. The meniscus is formed by condensing water. The contact angles were set equal to $\Theta_1 = \Theta_2 = \Theta = 0$, 20, and 40°. For the exact solutions, the following equations were applied:[26,29,43]

$$F = \pi\gamma R\sin\beta\left[2\sin(\beta + \Theta) + R\sin\beta\left(\frac{1}{r} - \frac{1}{l}\right)\right] \tag{16a}$$

$$r = \frac{R(1 - \cos\beta) + D}{\cos(\beta + \Theta) + \cos\Theta} \tag{16b}$$

$$l = R\sin(\beta - r)[1 - \sin(\beta + \Theta)] \tag{16c}$$

The angle β describes the position of the contact line of the liquid on the sphere (Figure 1). Practically, the parameter β was varied. For each β, values of r, l, F, and the overall curvature ($^1/_r - {}^1/_l$) were calculated. Using this curvature, the relative vapor pressure P/P_0 was calculated using the Kelvin equation. To derive eq 16, the shape of the meniscus was calculated with the toroidal approximation.[1,20]

Force versus distance curves calculated with eq 15 show a linear decrease (Figure 5). The slope is determined by the curvature r and thus the vapor pressure. With increasing contact angle, the capillary force decreases. The approximation in eq 15

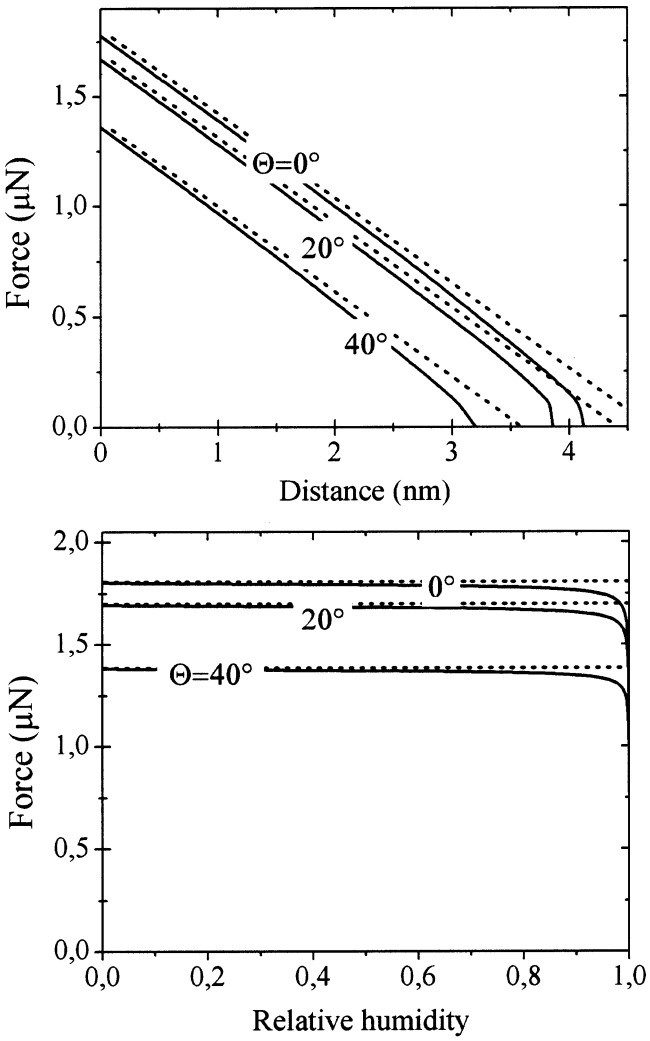

Figure 5. Capillary force for water between a sphere of radius $R = 2\,\mu$m and a plane for different contact angles ($\Theta_1 = \Theta_2 = 0$, 20, 40°). Continuous lines were calculated with eqs 16a−c using the full toroidal approximation. Dashed lines were calculated with eq 15. The capillary force was calculated with respect to distance at a humidity of 80% (top) and versus humidity at zero distance (bottom).

agrees well with the exact solutions in eq 16, except for large distances. At large distances, the liquid bridge will break, and the capillary force drops to zero at slightly smaller distances than predicted by eq 15. Some experiments show a longer range capillary force.[44,45] However, on the time scale of the experiment these are measured under constant-volume conditions, and the equilibrium required for Kelvin's equation to hold is not established.

The agreement between results obtained with eqs 15 and 16 also holds when considering the humidity dependence (bottom). In this case, I assumed that the two surfaces are in contact. Only at very high humidity does the exact solution predict a sharp decrease in the capillary force (see also refs 32 and 46) whereas eq 15 predicts a constant attraction. This humidity dependence is in clear contrast to experimental results. Experiments with particles[47−50] and atomic force microscope tips[28,33,51−55] showed

(42) Derjaguin, B. *Kolloid Z.* **1934**, *69*, 155−164.
(43) Cross, N. L.; Picknett, R. G. Particle Adhesion in the Presence of a Liquid Film; International Conference on the Mechanism of Corrosion by Fuel Impurities, Marchwood, England, 1963; Johnson, H. R., Littler, D. J., Eds.; Butterworths: Marchwood, England, 1963; pp 383−390.
(44) Mason, G.; Clark, W. C. *Chem. Eng. Sci.* **1965**, *20*, 859−866.
(45) Sprakel, J.; Besseling, N. A. M.; Leermakers, F. A. M.; Cohen-Stuart, M. A. *Phys. Rev. Lett.* **2007**, *99*, 104504.
(46) Pakarinen, O. H.; Foster, A. S.; Paajanen, M.; Kalinainen, T.; Katainen, J.; Makkonen, I.; Lahtinen, J.; Nieminen, R. M. *Model. Simul. Mater. Sci. Eng.* **2005**, *13*, 1175−1186.
(47) Fuji, M.; Machida, K.; Takei, T.; Watanabe, T.; Chikazawa, M. *J. Phys. Chem. B* **1998**, *102*, 8782−8787.

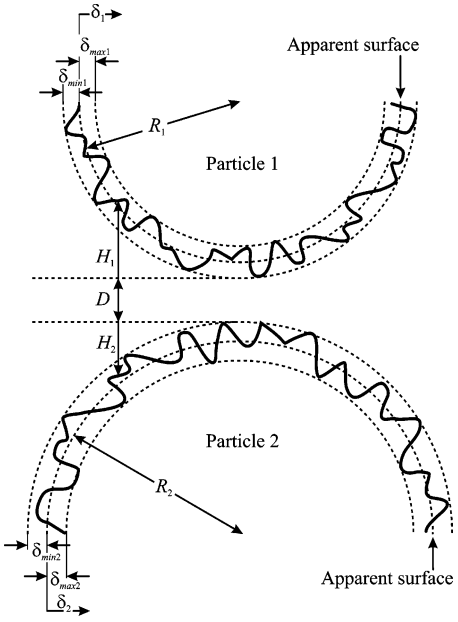

Figure 6. Schematic of two rough spheres interacting with each other. Symbols used in the text are indicated.

that at low and intermediate humidity the capillary forces increase with increasing humidity.

Roughness. When considering rough surfaces, it is useful to distinguish between two contributions: the apparent, nominally smooth shape and roughness. Let the height distribution of the apparent surface be described by g'. To take roughness into account, I introduce the distribution of asperity heights $\varphi_1(\delta_1)$ and $\varphi_2(\delta_2)$, where δ_1 and δ_2 are the deviations from the apparent surface height for surfaces 1 and 2 respectively. $\varphi_1(\delta_1)$ is the probability of finding a certain height value on surface 1 in the interval $\delta_1 \ldots \delta_1 + \mathrm{d}\delta_1$ above the reference plane. $\varphi_2(\delta_2)$ is the probability of finding a certain height value on surface 2 in the interval $\delta_2 \ldots \delta_2 + \mathrm{d}\delta_2$. The coordinates δ_1 and δ_2 can be negative (asperities) or positive (depressions) (Figure 6). In principle, φ_1 and φ_2 can be experimentally determined, for example, by atomic force microscopy or grazing incidence X-ray reflectivity. Functions φ_1 and φ_2 are in units of m^{-1} and they are normalized:

$$\int_{-\delta_{\min 1}}^{\delta_{\max 1}} \varphi_1(\delta_1)\,\mathrm{d}\delta_1 = 1 \text{ and } \int_{-\delta_{\min 2}}^{\delta_{\max 2}} \varphi_2(\delta_2)\,\mathrm{d}\delta_2 = 1 \quad (17)$$

Here, $\delta_{\min 1}$ and $\delta_{\min 2}$ are the maximal asperity heights, and $\delta_{\max 1}$ and $\delta_{\max 2}$ are the maximal depression depths, respectively. Asperity distribution functions $\varphi_1(\delta_1)$ and $\varphi_2(\delta_2)$ introduced here are more general than the distribution functions introduced by Greenwood and Williamson[35] because they allow for nonspherical asperities. However, I had to assume that the inclination of the surfaces should be low.

The joint asperity distribution is the convolution of the two asperity distributions

$$\varphi(\delta) = \int_{-\delta_{\min 1}}^{\delta_{\max 1}} \varphi_1(\delta_1)\,\varphi_2(\delta - \delta_1)\,\mathrm{d}\delta_1 = \int_{-\delta_{\min 2}}^{\delta_{\max 2}} \varphi_2(\delta_2)\,\varphi_1(\delta - \delta_2)\,\mathrm{d}\delta_2 \quad (18)$$

Here, $\varphi(\delta)$ with $\delta = \delta_1 + \delta_2$ is the probability of finding a certain height value in the interval $\delta \ldots \delta + \mathrm{d}\delta$. $\varphi(\delta)$ is defined in the interval between $-\delta_{\min}$ with $\delta_{\min} = \delta_{\min 1} + \delta_{\min 2}$ and $\delta_{\max} = \delta_{\max 1} + \delta_{\max 2}$. It is zero outside that range.

The integration endpoints of eq 18 were simply taken to be the sum of the individual distributions: $\delta_{\min} = \delta_{\min 1} + \delta_{\min 2}$ and $\delta_{\max} = \delta_{\max 1} + \delta_{\max 2}$. This is by no means always the case and may be modified depending on the special situation. The underlying assumption is that at contact the highest asperities of surfaces 1 and 2 meet. For infinitely extended, nondeformable, parallel surfaces, this is fulfilled. In practical cases, for example, for particles, the highest asperity on surface 1 might meet a depression on surface 2, and the highest asperity in the combined distribution can be smaller than $\delta_{\min 1} + \delta_{\min 2}$. At this point, the lateral distribution of asperities,[34] which I avoided discussing here and partially accounts for the simplicity of the theory, becomes relevant. I leave a detailed discussion of this matter for future work.

Two Parallel Plates. As an example, I consider two parallel plates of area A_0, whose roughness is described by a symmetric rectangular function $\varphi_1 = \varphi_2 = 1/\delta_0$ for $-\delta_0/2 < \delta_1 \le \delta_0/2$ and $-\delta_0/2 < \delta_2 \le \delta_0/2$. Outside of that range, $\varphi_1 = \varphi_2 = 0$. With

$$\varphi(\delta) = \int_{-\delta_0/2}^{\delta_0/2} \varphi_1(\zeta)\,\varphi_2(\delta - \zeta)\,\mathrm{d}\zeta \quad (19)$$

we find that

$$\varphi(\delta) = \frac{\delta_0 + \delta}{{\delta_0}^2} \text{ for } -\delta_0 \le \delta \le 0 \quad (20a)$$

$$\varphi(\delta) = \frac{\delta_0 - \delta}{{\delta_0}^2} \text{ for } 0 \le \delta \le \delta_0 \quad (20b)$$

$\varphi = 0$ for $\delta < -\delta_0$ or $\delta > \delta_0$.

Roughness for Arbitrary Bodies. The height distribution for two interacting rough surfaces is the convolution of g' and φ. If $H_{\max}$ is the maximal argument of g', then the combined height distribution g is given by

$$g(z) = \int_0^{H_{\max}} g'(\zeta)\,\varphi(\zeta - z)\,\mathrm{d}\zeta \quad (21)$$

where $-\delta_{\min} \le z \le H_{\max}$. The integrated height distribution is

$$G(z) = \int_{-\delta_{\min}}^{z - \delta_{\min}} g(\zeta)\,\mathrm{d}\zeta \quad (22)$$

In the endpoints of the interval of integration, I subtracted $\delta_{\min}$ to shift zero distance to the point where the highest asperities meet and define contact. The normalization is now $\int_{-\delta_{\min}}^{H_{\max}} q(z)\mathrm{d}z = 1$. After eq 22 is solved, the capillary force is given by eq 7.

Two Different Rough Spheres. As an example, I consider two rough spheres of different radii. The roughness of both individual surfaces is assumed to be described by the same rectangular height distribution according to eq 20. We set the upper limit of the height considered to $H_{\max} = R^*$. Because $R^* \gg \lambda_K$, forces outside that height will not contribute. A discrimination into three regimes is useful (Figure 7). For $-\delta_0 < z \le 0$,

$$g(z) = \frac{2}{{R^*}^2} \int_0^{z+\delta_0} (R^* - \zeta)\,\frac{(\delta_0 - \zeta + z)}{{\delta_0}^2}\,\mathrm{d}\zeta \quad (23)$$

(48) Biggs, S.; Cain, R. G.; Dagastine, R. R.; Page, N. W. *J. Adhes. Sci. Technol.* **2002**, *16*, 869−885.
(49) Jones, R.; Pollock, H. M.; Cleaver, J. A. S.; Hodges, C. S. *Langmuir* **2002**, *18*, 8045−8055.
(50) Young, P. M.; Price, R.; Tobyn, M. J.; Buttrum, M.; Dey, F. *J. Pharm. Sci.* **2003**, *92*, 815−822.
(51) Ando, Y. *Wear* **2000**, *238*, 12−19.
(52) Thundat, T.; Zheng, X. Y.; Chen, G. Y.; Warmack, R. J. *Surf. Sci. Lett.* **1993**, *294*, L939−L943.
(53) Xu, L.; Lio, A.; Hu, J.; Ogletree, D. F.; Salmeron, M. *J. Phys. Chem. B* **1998**, *102*, 540−548.
(54) Xiao, X.; Qian, L. *Langmuir* **2000**, *16*, 8153−8158.
(55) He, M.; Blum, A. S.; Aston, D. E.; Buenviaje, C.; Overney, R. M. *J. Phys. Chem.* **2001**, *114*, 1355−1360.

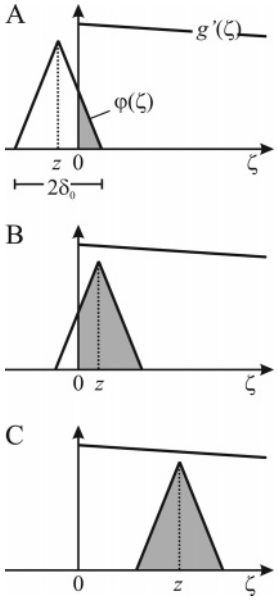

Figure 7. Schematic of the convolution of functions g' and φ for two similar rough spheres in the three regimes: $-\delta_0 < z \le 0$ (A), $0 \le z \le \delta_0$ (B), and $\delta_0 < z$ (C). The gray area indicates the convolution.

Taking into account that δ_0 and thus the maximal value of the integration variable ζ is much lower than R^*, we can simplify the integrand:

$$g(z) = \frac{2}{{\delta_0}^2 R^*} \int_0^{z+\delta_0} (\delta_0 - \zeta + z)\, d\zeta = \frac{(\delta_0 + z)^2}{{\delta_0}^2 R^*} \quad (24a)$$

Specifically, $g(0) = 1/R^*$. For $0 < z \le \delta_0$, we have

$$g(z) = \frac{2}{{\delta_0}^2 R^*} \int_0^{z} (\delta_0 + \zeta - z)\, d\zeta + \frac{1}{R^*} = \frac{1}{{\delta_0}^2 R^*} ({\delta_0}^2 + 2\delta_0 z - z^2) \quad (24b)$$

For $z > \delta_0$,

$$g(z) \approx \frac{2}{{R^*}^2}(R^* - z) \quad (24c)$$

The integrated height distribution is

$$G(z) = \int_{-\delta_0}^{z-\delta_0} \frac{(\delta_0 + \zeta)^2}{{\delta_0}^2 R^*}\, d\zeta = \frac{z^3}{3{\delta_0}^2 R^*} \text{ for } 0 \le z \le \delta_0 \quad (25a)$$

Specifically, $G(\delta_0) = \delta_0/3R^*$. For $\delta_0 \le z \le 2\delta_0$, we have

$$G(z) = \int_0^{z-\delta_0} \frac{{\delta_0}^2 + 2\delta_0\zeta - \zeta^2}{{\delta_0}^2 R^*}\, d\zeta + \frac{\delta_0}{3R^*} = \frac{1}{3{\delta_0}^2 R^*}[z^3 - 2(z - \delta_0)^3] \quad (25b)$$

and $G(2\delta_0) = 2\delta_0/R^*$. For $2\delta_0 < z \le H_{max}$,

$$G(z) = \frac{2}{{R^*}^2} \int_{\delta_0}^{z-\delta_0} (R^* - \zeta)\, d\zeta + \frac{2\delta_0}{R^*} = \frac{2}{{R^*}^2}\left[R^*(z - \delta_0) - \frac{z^2 - 2z\delta_0}{2}\right] \approx \frac{2(z - \delta_0)}{R^*} \quad (25c)$$

The force is obtained with eq 7 by inserting $A_0 = \pi {R^*}^2$ and $z = 2cr - D$.

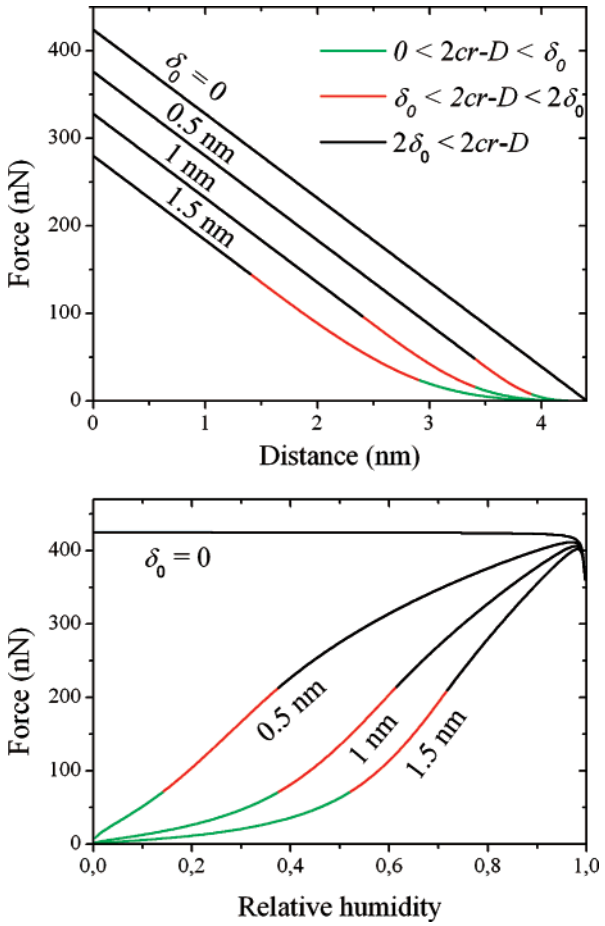

Figure 8. Capillary force for water between two equal spheres of radii $R = 1$ μm, a contact angle of $\Theta = 20°$, and roughnesses of $\delta_0 = 0$, 0.5, 1, and 1.5 nm, described by eq 20. The capillary force was calculated with respect to distance at a humidity of 80% and versus humidity at zero distance. Green lines were calculated using eq 7 with G determined by eq 26a, red lines determined by eq 26b, and black lines determined by eq 26c and $A_0 = \pi R^2$.

For two similar spheres, we could insert $R^* = R/2$ for the effective radius. However, it is more instructive to use $A_0 = \pi R^2$, which is the maximal cross-sectional area, as a reference. The integrated height distribution is then

$$G(z) = \frac{z^3}{6{\delta_0}^2 R} \text{ for } 0 \le z \le \delta_0 \quad (26a)$$

Specifically, $G(\delta_0) = \delta_0/6R$. For $\delta_0 \le z \le 2\delta_0$, we have

$$G(z) = \frac{1}{6{\delta_0}^2 R}[z^3 - 2(z - \delta_0)^3] \quad (26b)$$

and $G(2\delta_0) = \delta_0/R$. For $2\delta_0 < z \le H_{max}$,

$$G(z) = \frac{1}{R^2}[(R - z)(z - \delta_0) + z\delta_0] \approx \frac{z - \delta_0}{R} \quad (26c)$$

The force is obtained with eq 7 by inserting $A_0 = \pi R^2$.

Force versus distance and force versus vapor pressure curves depend sensitively on roughness. For two equal spheres of 1 μm radius and with a contact angle of 20° with respect to water in a humid atmosphere, this is demonstrated in Figure 8. For a smooth sphere ($\delta_0 = 0$), the capillary force decreases linearly with distance. This changes as soon as the surfaces show even a low roughness. The combined roughness, $\varphi(\delta)$, was assumed

to be described by eq 20 with $\delta_0 = 0.5$, 1, and 1.5 nm. The capillary force decreases, and at large distances the decrease is not linear anymore. Even more drastic is the change when considering capillary force versus humidity curves for the two spheres in contact. Rather than starting with a constant high force at low humidity, force versus humidity curves start at zero. The capillary force increases with humidity to reach a maximum close to $F = 2\pi\gamma R \cos \Theta$. This agrees with earlier, more exact calculations[32] and with the results of experiments with particles[47−50] or atomic force microscope tips.[28,33,51−55]

Summary

To calculate the capillary force for rough surfaces, the following formalism is suggested:

- Determine the height distribution function of the gap between the surfaces g', for example, by light or electron microscopy.
- Determine the combined asperity distribution function φ, for example, by atomic force microscopy or grazing incidence X-ray reflectometry.
- Convolute both functions according to eq 21 to obtain the combined height distribution function g.
- Integrate g to get the integrated height distribution function G according to eq 22.
- Multiply G by the chosen reference cross-sectional area A_0 and by the Laplace pressure γ/r to obtain the capillary force (eq 7).

Assumptions are that the lateral extension of the menisci formed is much larger than the separation normal to the surfaces, that the inclination of the apparent surfaces is low, and that the liquid menisci are in equilibrium with their vapor. Capillary forces calculated with this formalism agree with more exact calculations and experimental results on the adhesion between particles. To include the effect of surface heterogeneity, replacing the height distribution by the height distribution divided by the mean of the cosine of the local contact angles is suggested.

Acknowledgment. I thank the DFG TR6 for supporting this project.

LA703640F